# Towards fast assessment of kidney structure and function from DCE-MRI

Project report

Katarzyna Sprawka
Under supervision of Prof. Arvid Lundervold
in collaboration with Alexander Lundervold


Department of Biomedicine
University of Bergen, Norway

December 21, 2017

# Contents

**Contents** **2**

**1 Introduction** **3**

1.1 Glomelural Filtration Rate . . . . . 4

1.2 DCE-MRI of the kidneys . . . . . 5

1.3 Aim of the overall project . . . . . 5

**2 Methods** **6**

2.1 DCE-MRI data acquisition . . . . . 6

2.2 Motion correction . . . . . 6

2.3 Manual labelling of kidneys and aorta . . . . . 6

2.4 Pelvis segmentation . . . . . 6

2.4.1 Dimensionality reduction . . . . . 7

2.4.2 Clustering . . . . . 7

2.5 Kidneys segmentation using deep learning . . . . . 7

2.6 Pharmacokinetic modelling . . . . . 9

2.6.1 Concentration time courses . . . . . 9

2.6.2 Toft's model . . . . . 11

2.6.3 Extended Toft's model . . . . . 11

2.6.4 Patlak plot . . . . . 11

2.6.5 GFR estimation . . . . . 12

**3 Results** **14**

**4 Conclusions** **15**

**5 Summary** **16**

**References** **17**

**Appendices** **20**

**Abstract**

.

.

.

.

.

.

.

.

.

.

.

.

.

# 1. Introduction

Kidneys, although often underestimated, are fundamental organs of human body and their working mechanism is extremely complex. Their essential task is to remove wastes from the organism but their functionality is much wider. They are also involved in maintaining acid-based balance, regulating the blood pressure and are major endocrine organs, which secret three important hormones: erythropoietin, calcitriol and renin. Besides the production, they also take part in degradation of hormones such as insulin or parathyroid hormon [1]. The basic functional units of the kidney are nephrones. Above million of them enables it to perform above functions [2].

Anatomically, kidney can be divided into three main parts: (1) renal cortex, which is the outer part of the kidney (2) medulla, the inner part of the kidney composed of medullary pyramids (3) pelvis, the extension of the ureter, which collects the urine [1, 2]. The structure of the kidney is shown on Figure 1.

Kidneys are responsible for maintaining homeostasis of all body due to which, all organs can work in optimal environment. It is crucial for proper functioning of whole organism [3]. One can conclude that the role of kidneys is enormously important.

Gradually progressing loss of kidney function known as a chronic kidney desease is a growing world-wide problem. As much as 8–16% of whole population suffers from this condition [4]. It significantly decreases comfort of life and in extreme cases leads to death. What is more, it was shown that renal diseases are risk factor for development of cardiovascular diseases [5]. Because of the fact that symptoms don't resemble renal failure, approximately 90% of the ill are unconscious of it until late stages [6]. That is way there is the demand for methods, which enable fast and accurate measurement of renal function required for all of three: prevention, monitoring and therapy.

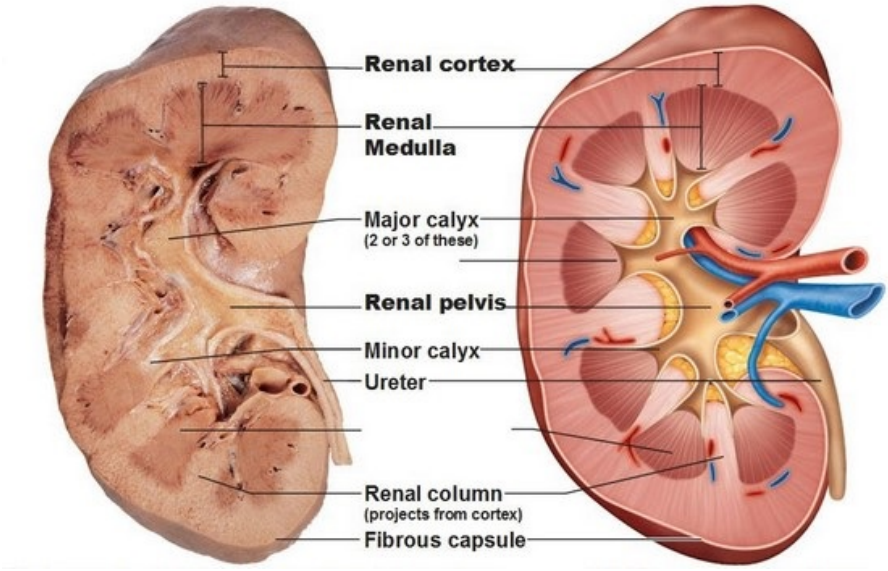


**Figure 1:** *Anatomy of the kidney [1].*

## 1.1. Glomelural Filtration Rate

The metrics of level of kidney function is glomelural filtration rate (GFR) [7]. Not only does it allow for assessment how well our kidneys are working, but also it can determine the stage of kidney disease. In short terms, it is the volume of fluid filtered from the renal glomerular capillaries into the Bowman's capsule per unit time [8]. GFR measurement is of great clinical importance and is crucial for diagnosis and management of renal diseases. The GFR in healthy adult kidney is equal approximately 90–130 mL/min/1.73 $m^2$ [9]. Lower at birth, it approaches its adult value at the age two and maintains its level till the age of fourty, when it starts decreasing again [10].

The classical method of GFR measurement incorporates injection of the exogenous marker that is freely filtered by the kidney, and that does not undergo metabolism, tubular secretion or absorption. An example of such a marker can be insulin, ohexol or iothalamate. Even thought this method is considered the gold standard in GFR measurement, because of its limitations, it is not a clinical routine if very accurate measurements are not required. This special cases include transplant donors or scientific research [7]. Other, more frequently used techniques involve using endogenous markers such a creatinine or urea and estimating GFR applying validated algoritms [11].

Although described methods allow for sufficiently accurate GFR estimation or even exact measurement, they are not very practical in clinical use. Not only are they time-consuming and expensive but also they can be cumbersome. What is more they cannot be used for single kidney function assessment and thus other methods are desired [12].

## 1.2. DCE-MRI of the kidneys

An innovative approach in estimating renal function is performing dynamic contrast-enhanced magnetic resonance (DCE-MRI). During the examination a contrast agent is injected into the blood and the T1-weighted images are acquired. The passage of the tracer through the kidney results in changes in signal intensities over the time. The analysis of the obtained time-intensity changes as a function of time provides important functional information [12, 13]. Traditionally, this evaluation is performed by experienced observer, although this method is very subjective and strongly depends on the experience of the expert. Other technique involves fitting tissue intensity changes to pharmacokinetic models, which allows quantification of renal function [13]. Even though this strategy is gaining more and more supporters, most of the methods still require interference of the human at some stage, which makes them vulnerable to human factors.

## 1.3. Aim of the overall project

The overarching aim of this project is to develop entirely data-driven method of GFR estimation directly from DCE-MRI, which would be fast and efficient and accurate enough to be used it clinical applications.

# 2. Methods

## 2.1. DCE-MRI data acquisition

The data used in this project were acquired on 32 channel 1.5 T whole-body scanner (Siemens Magnetom Avanto [14]). The images covering kidneys and aorta were continuously acquired every 2.3 s for approximately 6 min in coronal-oblique plane. Each of 74 time volumes consisted of 30 slices. The aquisition matrix was 192x192 whereas the voxel size was equal to 2.2x2.2x3 $mm^3$ More information about aquisition of DCE-MRI data used in this project can be found in [15].

## 2.2. Motion correction

One of the first fundamental problem encountered during DCE-MRI analysis is misalignment of 3D volumes across time slices. This misalignment of organs is a result of the patiens's respiratory motion as well as the heartbeat and bowel peristalsis and is unavoidable during examination. Studies have shown that even slight misalignment can lead to significant differences in intensity time-courses [16] and thus, motion correction of time series is essential for further analysis.

In order to remove motion artifact, all files were motion-corrected across time points. For this purpose R programming language for statistical computing and graphics was used [17] together with the package ANTsR [18], which provides quantification tools for biomedical images. As an initial step, for every time series, the algorithm extracted 3D volumes. Each extracted volume corresponded to data obtained in one time point. Next, the average image of the temporal volumes was calculated, which was treated as a mask for image registration. Every temporal volume was then aligned to the mask and at the end they were combined back together into 4D time series.

## 2.3. Manual labelling of kidneys and aorta

In the next step, labels of both left and right kidney were created. For this purpose, 3D volumes were extracted for every time frame and the image with maximal signal enhancement was chosen (usually between 12–17 time slice). On this image, left and right kidney were manually delineated in coronal plane using ITK-Snap software [19]. Additionally, few voxels of aorta (15–20) were labelled. So obtained labels were then propagated across the time points. All further analysis was implemented in Python programming language v. 3.6 [20].

## 2.4. Pelvis segmentation

Due to the fact that glomelular filtration takes place in renal renal parenchyma, pelvis had to be removed from further analysis.

Resulting from the physiology of the process, the three renal compartments (cortex, medulla, pelvis) can be distinguished from each other on the basis of their time courses, as shown on Figure 2. Depending on the compartment, the rapid enhancement of the signal occurs in different period, which makes the shapes of the time intensity curves very unique. From the 2 it can be seen that the biggest variation is observed between pelvis and two other renal compartments. Consequently, it can be separated by unsupervised clustering.

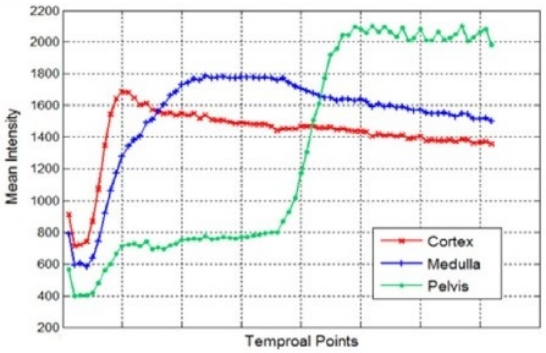


**Figure 2:** *Kidney compartments timecourses [16].*

#### 2.4.1. Dimensionality reduction

Raw DCE-MRI data usually has high dimension, which results in computational complexity, and thus memory and time consumption as well as numerical problems. What is more it contains a lot of noises [16]. To overcome this problems, the Principal Component Analysis (PCA) [21] was applied.

PCA is a statistical procedure, which transforms the number of related features into smaller set of uncorrelated variables [22]. These so called principal components (PCs) are a linear combination of the original variables [23]. As a result, after rotating the feature space, the first PC contains most variance and so on. In this way the dominant patterns are extracted while the noises are reduced [21].

Applying the theory to practice, each voxel belonging to the kidneys, initially described by 74 features (value of the signal intensity in 74 time points) was described by 10 PCs.

#### 2.4.2. Clustering

In the next step, the k-means clustering [24] was performed in order to separate voxels into two groups: pelvis and renal parenchyma.

The k-means is an unsupervised clustering algorithm aiming to minimize the square error function given by:

$$J = \sum_{j=1}^{k} \sum_{i=1}^{n} (||x_i - c_j||)^2, \tag{2.1}$$

where $||x_i - c_j||$ is the Euclidean distance between a data point $x_i$ and the cluster centre $c_j$ of k predefined clusters.

For each of two clusters, in which signal intensity reaches its maximum $T_{max}$ was calculated. Following the assumption that $T_{max\_pelvis} > T_{max\_parenchyma}$, the cluster with greater $T_{max}$ was marked as the pelvis and removed from the region of interest (ROI).

### 2.5. Kidneys segmentation using deep learning

As mentioned before, the main goal of the overall project is to develop method not requiring the interference of the human at any stage and thus being fully objective, which is contrary with previously described steps. In target method, the steps descried in sections 2.3 - 2.4 will be replaced by deep learning techniques. The designed neural networks should not require registration of the images, which is usually the most inconvenient step. Not only is it very time-consuming (motion correction of the one time series used in the project lasts ~6h) but also it causes loss of information. As a result, the method will enable fast and efficient automated GFR estimation directly from the DCE-MRI without any previous preprocessing. Although applying deep learning is still under intensive development, current studies already have showed promising results. What was achieved so far, is segmentation of the both left and right kidney from raw DCE-MRI images using convolutional neural network.

Convolutional Neural Networks (CNN) were inspired by the architecture of the animal visual cortex and are specifically suitable for image recognition. It was shown that numerous neurons in the visual cortex are sensitive only to the stimuli located in the small limited region of the visual field. In short terms, these neurons have small local receptive fields, which can overlap and all together cover whole visual field. What is more, certain neurons are activated only by horizontal lines, whereas the others reacts to these of different orientations. Furtermore, some neurons with bigger receptive fields responds to the more complex patterns being the assembly of the lower-level patterns, which leads to the conclusion that the higher-level neurons are based on the outputs of neighbouring lower-level neurons [25, 26]. The described complex system composed of the neurons ordered in a columnar fashion is able to detect all kinds of patterns in whole visual field creating the visual perception. The above idea is shown on Figure 3.

From the finding of the studies on visual cortex convolutional neural networks emerged. Unlike the traditional neural networks, their architecture incorporates multiple convolutional layers, neurons of which connect to the subregions of the previous layers instead of being fully-connected. The neurons are not sensitive to the areas outside of these subregions in the image. Each of the layer learn to recognise different feature. The deeper the layer is, the more detailed

The network has a dual pathway architecture incorporating both local and global information in the volumes. It consist of (?) layers. The idea of transfer learning was applied.

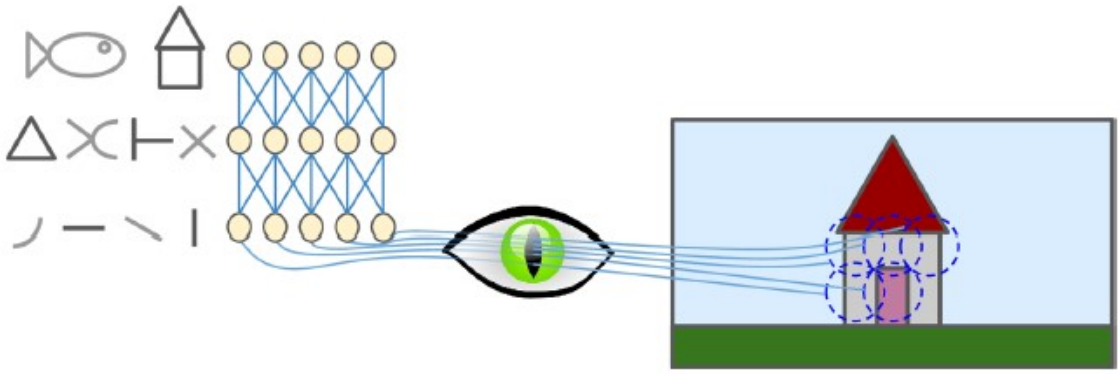

**Figure 3:** *Local receptive fields in the visual cortex [26].*

## 2.6. Pharmacokinetic modelling

The time-dependent distribution and disposition of a substance in a living system can be described by phamacokinetic (PK) models [27]. They aim to characterise a physiologic system by decomposing them into interacting compartments. Every of them is a homogenous, well-mixed space with the uniform tracer distribution [28].

PK models have very wide clinical application: from estimating the optimal drug dose to determining safe working environment while working with toxins [27]. Given the fact that the contrast agent used in DCE-MRI examination can be considered as a substance flowing through the organism, pharmacokintetic modelling can also be used in analysis of so obtained data. This approach, called the parametric one, is based on fitting mathematical model to acquired tissue concentration time courses. In this way, the quantitative parameters can be assessed, which cannot be overestimated while evaluating the renal function.

The compartment PK models decribe complex blood-tissue exchanges and their theory is based on the differential mass balance equations [29]. An example of the system decribed by two compartments is presented on Figure 5.

### 2.6.1. Concentration time courses

All PK models used during DCE-MRI analysis require determining both the tissue, $C_t(t)$, and blood plasma, $C_p(t)$, concentration as a function of time. In our case, the $C_t(t)$ is the mean concentration in renal parenchyma, whereas the $C_p(t)$, or so called arterial input function (AIF), is a concentration in a blood vessel feeding the kidney (aorta) [13].

For each of the kidney, as well as for the aorta, the mean intensities in each time point were calculated. Assuming the linear relation between tracer concentration and signal intensity $S(t)$ [30], the tracer concentration can be expressed as:

$$C(t) = S(t) - S(0), \tag{2.2}$$

where $S(0)$ is the baseline signal. In order to determine S(0), the time point before rapid signal drop had to be found as marked on Figure 6.

**First method:** To do so, for the time course under analysis, the time point in which the derivative of the function reaches the maximal

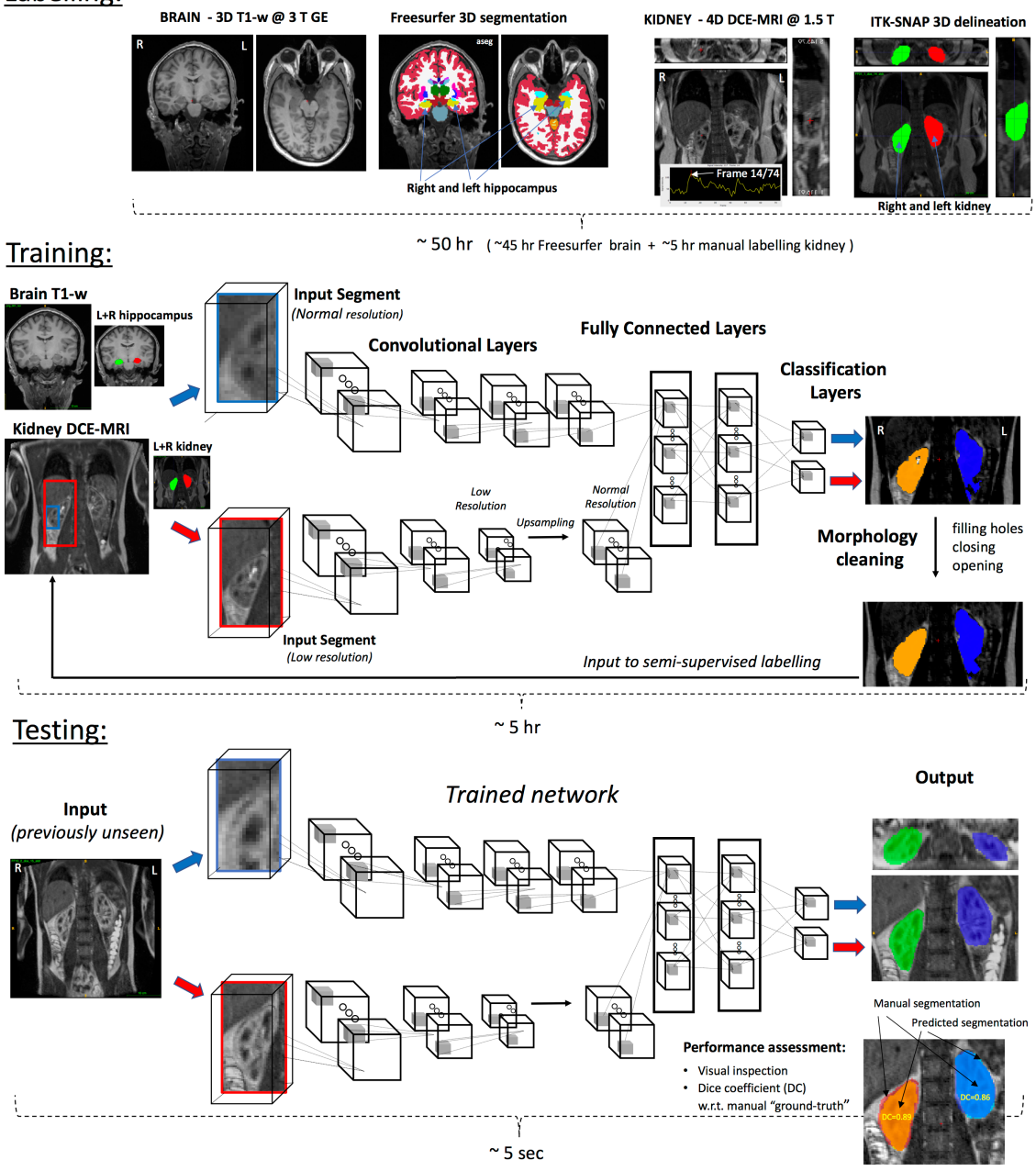
Labelling:
BRAIN - 3D T1-w @ 3 T GE
Freesurfer 3D segmentation
KIDNEY - 4D DCE-MRI @ 1.5 T
ITK-SNAP 3D delineation
Right and left hippocampus
Frame 14/74
Right and left kidney
~ 50 hr ( ~45 hr Freesurfer brain + ~5 hr manual labelling kidney )
Training:
Brain T1-w
L+R hippocampus
Input Segment
(Normal resolution)
Convolutional Layers
Fully Connected Layers
Classification Layers
Kidney DCE-MRI
L+R kidney
Low Resolution
Upsampling
Normal Resolution
Morphology cleaning
filling holes
closing
opening
Input Segment
(Low resolution)
Input to semi-supervised labelling
~ 5 hr
Testing:
Input
(previously unseen)
Trained network
Output
Manual segmentation
Predicted segmentation
Performance assessment:
Visual inspection
Dice coefficient (DC)
w.r.t. manual "ground-truth"
DC=0.86
~ 5 sec

**Figure 4**

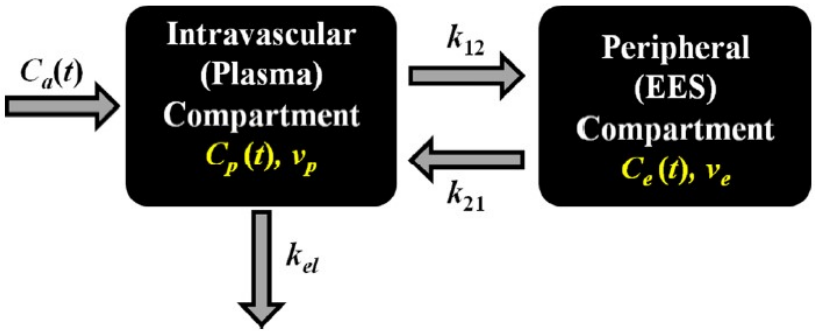


**Figure 5:** *An example two compartment model [13].*

value was selected.

**Second method:** To do so, for the time course under analysis, time point in which the function reaches the first local minimum $S_{local\_min}$ such that:

$$S_{local\_max} - S_{local\_min} > T_{baseline}, \tag{2.3}$$

where $S_{local\_max}$ is the first local maximum occurring after $S_{local\_min}$ and $T_{baseline}$ is threshold empirically set to 15 and 30 for the parenchymal volume and AIF respectively. $S(0)$ was then calculated as the mean signal intensity in the initial time interval starting at $T = 0$ to the determined point.

Obtained time-concentration curves were then fitted to the described in the next sections PK models.

### 2.6.2. Toft's model

The two compartment Toft's model [31] assuemes the diffusion of the tracer from the blood plasma at rate specified by the transfer constant $K_{trans}$ $(min^{-1})$ and returns at the rate $k_{ep} = K_{trans}/v_e$ $(min^{-1})$. In this model the assumption $C_t(t) = v_e C_e(t)$ is made, which means that plasma contribution is neglected. The blood plasma concentration $C_p$ is specified by AIF. According to the Toft's model the CA concentraion is specified by the formula:

$$C_t(t) = K_{trans} \int_0^t C_p(t') e^{-(K_{trans}/v_e)(t-t')} dt' \tag{2.4}$$

### 2.6.3. Extended Toft's model

While the Toft's model neglects intravascular contribution assuming weak vascularization of the tissue, the Extended Toft's model **??** does take it into account. The tissue concentration is described by the formula:

$$C_t(t) = v_p C_p(t) + \\ + K_{trans} \int_0^t C_p(t') e^{-(K_{trans}/v_e)(t-t')} dt', \tag{2.5}$$

where $v_p$ is the fractional plasma volume.

In Toft's and extended Toft's models the free parameters $K_{trans}$, $v_e$ and $v_p$ are estimated by fitting the model to obtained in DCE-MRI examinations time concentration curves.

### 2.6.4. Patlak plot

Another proposed approach is the graphical one called Patlak plot [32]. Patlak plot neglects

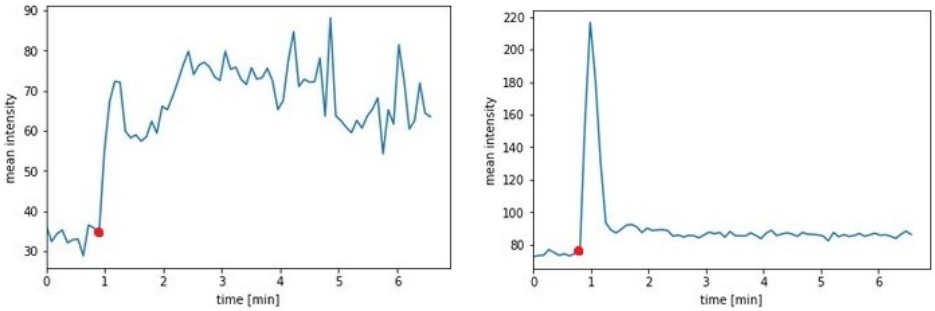


**(a)** *Kidney time course* **(b)** *Aorta time course*

**Figure 6:** *Sample average time-courses for renal parenchyma (a) and aorta (b). The last point of baseline is marked with red dot.*

$k_{ep}$ due to the low permeability and short examination time. As a result tissue concentration is expressed as:

$$C_t(t) = v_p C_p(t) + K_{trans} \int_0^t C_p(t')dt' \quad (2.6)$$

The above equation is the linearised as:

$$Y = K_{trans} X + v_p, \quad (2.7)$$

where $Y = C_t(t)/C_p(t)$ and $X = \int_0^t C_p(t')dt'/C_p(t)$. The free parameters $K_{trans}$ an $v_p$ can be then estimating by constructing a linear plot and calculating its slope and intercept respectively.

### 2.6.5. GFR estimation

Having calculated the $K_{trans}$ parameter the glomelural filtration rate can be computed according to the formula:

$$GFR = K_{trans} V_{parenchyma}(1 - H_{ct}) \quad (2.8)$$

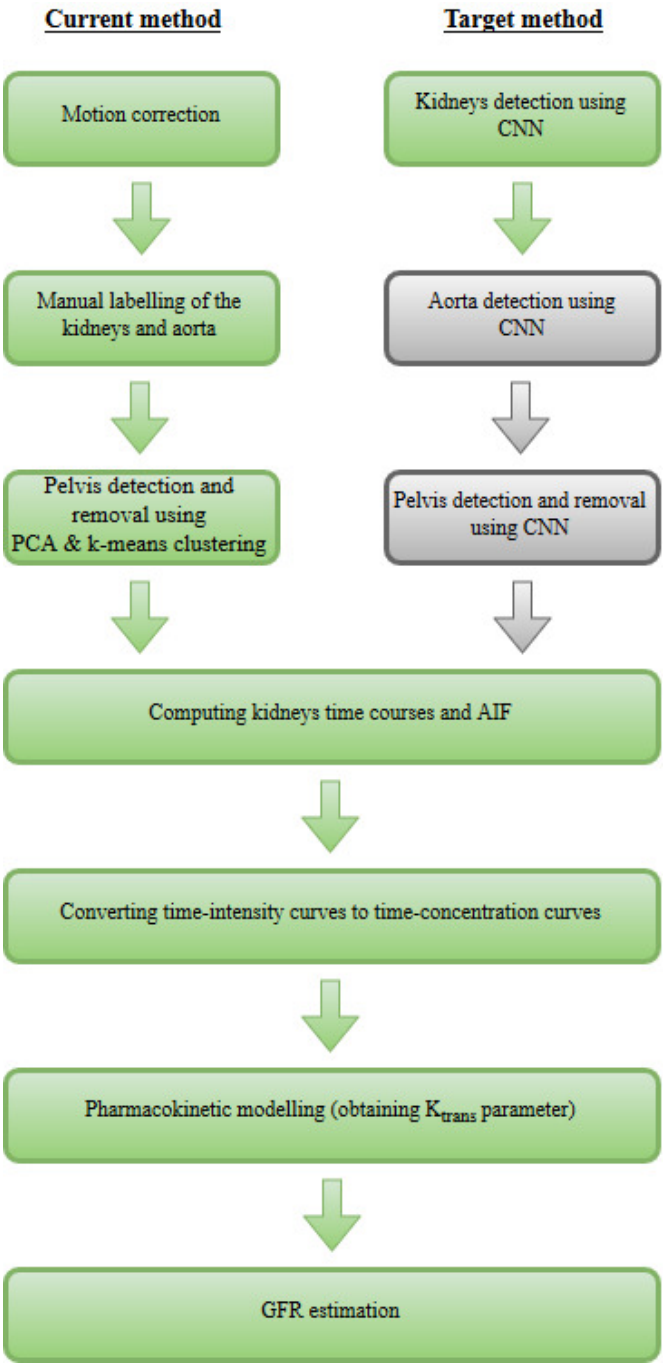
Current method
Target method
Motion correction
Kidneys detection using CNN
Manual labelling of the kidneys and aorta
Aorta detection using CNN
Pelvis detection and removal using PCA & k-means clustering
Pelvis detection and removal using CNN
Computing kidneys time courses and AIF
Converting time-intensity curves to time-concentration curves
Pharmacokinetic modelling (obtaining $K_{trans}$ parameter)
GFR estimation

**Figure 7**

# 3. Results

The segmentation of the pelvis was evaluated with Dice similarity coefficient given by the formula:

$$DS = \frac{2|A}{}, \tag{3.1}$$

where $||x_i - c_j||$ is the Euclidean distance between a data point $x_i$ and the cluster centre $c_j$ of k predefined clusters. The segmentation of the pelvis obtained for the sample kidney is shown on the Figure 8.

The example of the time concentration curves after baseline removal for the kidney and aorta are shown on Figure 9.

Fitting of the time course for different pharmacokinetic models is illustreted on the Figure 10.

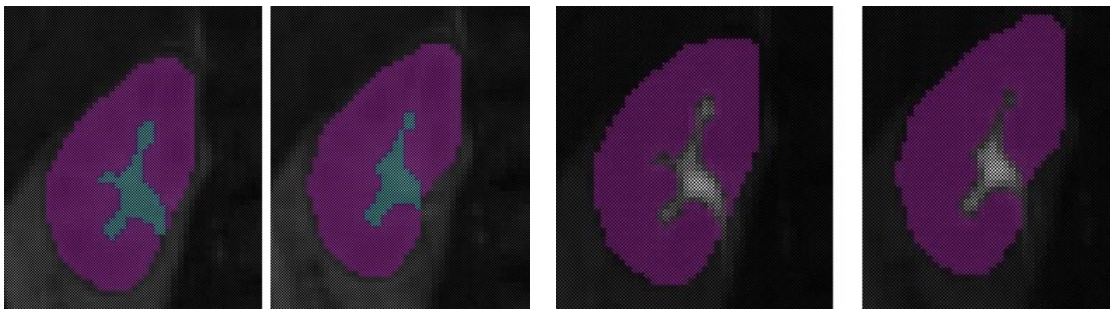

**(a)** *Segmented kidney* **(b)** *Parenchymal volume*

**Figure 8:** *The sample segmented kidney (a) and parenchymal volume with removed pelvis (b) purple - renal parenchyma, blue - renal pelvis.*

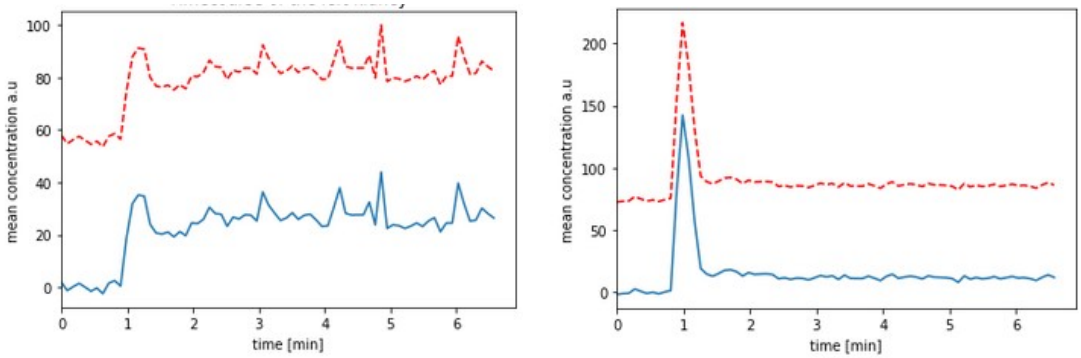


**(a)** *Kidney time course* **(b)** *Aorta time course*

**Figure 9:** *Sample average time-concentration curves for renal parenchyma (a) and aorta (b). The red curve shows the original data while the blue one - after baseline removal.*

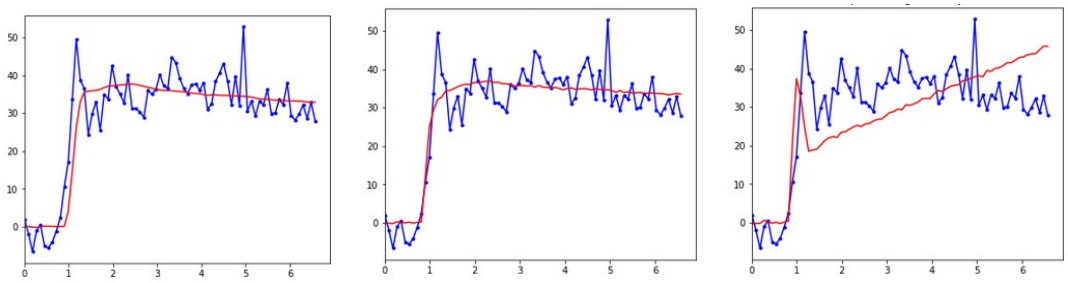

**(a)** *Toft's model* **(b)** *Extended Toft's model* **(c)** *Patlak model*

**Figure 10:** *Fit of the time-concentration curve of sample kidney to three different PK models.*

# 4. Conclusions

# 5. Summary

# References

[1] K. Saladin, *Anatomy & Physiology: The Unity of Form and Function*. USA: McGraw-Hill, 5th ed., 2009.

[2] K. Patton and G. Thibodeau, *The Human Body in Health & Disease*. USA: Elsevier, 7th ed., 2017.

[3] B. M. Koeppen and B. A. Stanton, *Renal Physiology: Mosby Physiology Monograph Series*. USA: Elsevier-Health Sciences Division, 5th ed., 2013.

[4] V. Jha, G. Garcia-Garcia, K. Iseki, Z. Li, S. Naicker, B. Plattner, R. Saran, A. Y.-M. Wang, and C.-W. Yang, "Chronic kidney disease: global dimension and perspectives," *The Lancet*, vol. 382, no. 9888, pp. 260–272, 2013.

[5] M. J. Sarnak, A. S. Levey, A. C. Schoolwerth, J. Coresh, B. Culleton, L. L. Hamm, P. A. McCullough, B. L. Kasiske, E. Kelepouris, M. J. Klag, *et al.*, "Kidney disease as a risk factor for development of cardiovascular disease," *Circulation*, vol. 108, no. 17, pp. 2154–2169, 2003.

[6] National Kidney Foundation, "Kidney disease: the basics." [Online]. Available: https://www.kidney.org/news/newsroom/factsheets/KidneyDiseaseBasics. [Accessed: 13-Nov- 2017].

[7] J. Traynor, R. Mactier, C. C. Geddes, and J. G. Fox, "How to measure renal function in clinical practice," *BMJ: British Medical Journal*, vol. 333, no. 7571, p. 733, 2006.

[8] The Free Dictionary: medical dictionary, "Glomerular filtartion rate." [Online]. Available: https://medical-dictionary.thefreedictionary.com/glomerular+filtration+rate. [Accessed: 13-Nov- 2017].

[9] H. W. Smith, *The kidney: structure and function in health and disease*, vol. 1. Oxford University Press, USA, 1951.

[10] J. R. Weinstein and S. Anderson, "The aging kidney: physiological changes," *Advances in chronic kidney disease*, vol. 17, no. 4, pp. 302–307, 2010.

[11] P. Delanaye, "How measuring glomerular filtration rate? comparison of reference methods," in *Basic Nephrology and Acute Kidney Injury*, InTech, 2012.

[12] L. Bokacheva, H. Rusinek, J. L. Zhang, and V. S. Lee, "Assessment of renal function with dynamic contrast-enhanced mr imaging," *Magnetic resonance imaging clinics of North America*, vol. 16, no. 4, pp. 597–611, 2008.

[13] F. Khalifa, A. Soliman, A. El-Baz, M. Abou El-Ghar, T. El-Diasty, G. Gimel'farb, R. Ouseph, and A. C. Dwyer, "Models and methods for analyzing dce-mri: A review," *Medical physics*, vol. 41, no. 12, 2014.

[14] Simens Healthineers, "Magnetom avanto." [Online]. Available: https://www.healthcare.siemens.com/magnetic-resonance-imaging/0-35-to-1-5t-mri-scanner/magnetom-avanto [Accessed: 13- Nov- 2017].

[15] E. Eikefjord, E. Andersen, E. Hodneland, E. A. Hanson, S. Sourbron, E. Svarstad, A. Lundervold, and J. T. Rørvik, "Dynamic contrast-enhanced mri measurement of renal function in healthy participants," *Acta Radiologica*, vol. 58, no. 6, pp. 748–757, 2017.

[16] X. Yang, H. Le Minh, K.-T. T. Cheng, K. H. Sung, and W. Liu, "Renal compartment segmentation in dce-mri images," *Medical image analysis*, vol. 32, pp. 269–280, 2016.

[17] R Development Core Team, *R: A Language and Environment for Statistical Computing*. R Foundation for Statistical Computing, Vienna, Austria, 2008. ISBN 3-900051-07-0.

[18] B. B. Avants, B. M. Kandel, J. T. Duda, P. A. Cook, N. J. Tustison, and S. KL, *ANTsR: ANTs in R: quantification tools for biomedical images*, 2016. R package version 0.3.3.

[19] P. A. Yushkevich, J. Piven, H. Cody Hazlett, R. Gimpel Smith, S. Ho, J. C. Gee, and G. Gerig, "User-guided 3D active contour segmentation of anatomical structures: Significantly improved efficiency and reliability," *Neuroimage*, vol. 31, no. 3, pp. 1116–1128, 2006.

[20] Python Core Team, *Python: A dynamic, open source programming language*. Python Software Foundation, 2015.

[21] S. Wold, K. Esbensen, and P. Geladi, "Principal component analysis," *Chemometrics and intelligent laboratory systems*, vol. 2, no. 1-3, pp. 37–52, 1987.

[22] J. E. Jackson, *A user's guide to principal components*, vol. 587. John Wiley & Sons, 2005.

[23] G. H. Dunteman, *Principal components analysis*. No. 69, Sage, 1989.

[24] J. MacQueen *et al.*, "Some methods for classification and analysis of multivariate observations," in *Proceedings of the fifth Berkeley symposium on mathematical statistics and probability*, vol. 1, pp. 281–297, Oakland, CA, USA., 1967.

[25] D. H. Hubel and T. N. Wiesel, "Receptive fields and functional architecture of monkey striate cortex," *The Journal of physiology*, vol. 195, no. 1, pp. 215–243, 1968.

[26] A. Géron, *Hands-On Machine Learning with Scikit-Learn and TensorFlow*. USA: O'Reilly Media, 2017.

[27] L. E. Gerlowski and R. K. Jain, "Physiologically based pharmacokinetic modeling: principles and applications," *Journal of pharmaceutical sciences*, vol. 72, no. 10, pp. 1103–1127, 1983.

[28] S. Sourbron, "Compartmental modelling for magnetic resonance renography," *Zeitschrift fur medizinische Physik*, vol. 20, no. 2, p. 101—114, 2010.

[29] S. Sourbron and D. L. Buckley, "Tracer kinetic modelling in mri: estimating perfusion and capillary permeability," *Physics in medicine and biology*, vol. 57, no. 2, p. R1, 2011.

[30] S. W. Lim, C. Chrysochou, D. L. Buckley, P. A. Kalra, and S. P. Sourbron, "Prediction and assessment of responses to renal artery revascularization with dynamic contrast-enhanced magnetic resonance imaging: a pilot study," *American Journal of Physiology-Renal Physiology*, vol. 305, no. 5, pp. F672–F678, 2013.

[31] P. S. Tofts and A. G. Kermode, "Measurement of the blood-brain barrier permeability and leakage space using dynamic mr imaging. 1. fundamental concepts," *Magnetic resonance in medicine*, vol. 17, no. 2, pp. 357–367, 1991.

[32] C. S. Patlak, R. G. Blasberg, and J. D. Fenstermacher, "Graphical evaluation of blood-to-brain transfer constants from multiple-time uptake data," *Journal of Cerebral Blood Flow & Metabolism*, vol. 3, no. 1, pp. 1–7, 1983.

# Appendices

## **Appendix A:** The abstract accepted for ECR (the European Congress of Radiology)


Print this Page for Your Records  Close Window

**Control/Tracking Number:** 18-P-3245-ECR
**Activity:** Scientific Paper (talk: 6min.+ 2min. discussion)
**Current Date/Time:** 10/8/2017 6:43:34 AM

**Fast estimation of kidney volumes and time courses in DCE-MRI using convolutional neural networks**

**Author Block:** A.S. Lundervold[1], K. Sprawka[2], A. Lundervold[1]; *[1]Bergen/NO, [2]Lodz/PL*

**Abstract:**
**Purpose:** We create a novel method for fast and accurate estimation of kidney volumes and signal intensity time-courses in DCE-MRI, aiming at extracting both structural and functional quantitative information from the moving kidney.
**Methods and Materials:** Two repeated SPGR-DCE-MRI datasets were acquired from 20 healthy volunteers, resulting in 40 examinations, each consisting of 74 volumes recorded over ~6 min. We trained a 3D convolutional neural network (using a single standard NVIDIA GeForce 1080Ti GPU) for segmentation of left and right kidneys. The network has a dual pathway architecture, incorporating both local and global information in the volumes. To create training data, we manually delineated 10 individual volumes from 10 different time-series, and extended the delineations to 740 volumes using image registration.
**Results:** Our implementation is able to segment all 74 volumes in a previously unseen, unregistered recording in less than 7 minutes. Mean segmentation accuracy (Dice) was 0.843 (SD=0.010). Mean (SD) left and right kidney volumes [ml] (incl. renal hilum) in one of the subjects (FF03) examined seven days apart (MR1 and MR2) was: MR1 L: 301.6 (15.9), R: 389.8 (16.9); MR2 L: 307.4 (17.8) R: 395.3 (23.6).
**Conclusion:** A CNN is able to quickly and accurately segment the moving kidneys in DCE-MRI, providing estimates of kidney volumes and mean signal intensity time courses. We are currently working to achieve sub-segmentation of the kidney (cortex, medulla, pelvis) and segmentation of the aorta (for AIF), enabling automated and fast estimation of GFR directly from the DCE-MRI.
**:**

Author Disclosure Information:

**A.S. Lundervold:** None. **K. Sprawka:** None. **A. Lundervold:** None.
**Invest in the Youth (Complete)**: No
**MyT3 Scientific Session (Complete)**:
: Disagree

**Topic (Complete)**: Imaging Informatics
**Additional Information (Complete)**:
***I understand that only digital projection material will be allowed:**
Yes
***I agree that the email address of the presenting author will be published within the ECR 2018 Book of Abstracts:**
Yes

**Abstract Categories (Complete)**:
**Areas of Interest**: Kidney
**Imaging Technique**: MR
**Procedure**: Computer Applications-Detection, diagnosis
**Procedure**: Segmentation

**Status:** Complete

## **Appendix B:** The code implemented for pharmacokinetic modelling

Under cleaning